Biointerface Research in Applied Chemistry
Open-Access Journal (ISSN: 2069-5837)

Article
Volume 14, Issue 1, 2024, 24
https://doi.org/10.33263/BRIAC141.024

Heat Transport Efficiency of Magnetized $AA7072/H_2O$ Nanofluid and $AA7072 + AA7075/H_2O$ Hybrid Nanofluid Past a Non-Linear Porous Stretching Sheet

Shanmugapriya Marayanagaraj [1], Sundareswaran Raman [1], Abdu Alameri [2,*]

[1] Department of Mathematics, Sri Sivasubramaniya Nadar College of Engineering, Chennai - 603 110, India; shanmugapriyam@ssn.edu.in (M. S.); sundareswaranr@ssn.edu.in (R. S.);
[2] Department of Biomedical Engineering, Faculty of Engineering, University of Science and Technology, Sana'a, Yemen; a.alameri2222@gmail.com (A.A.);
* Correspondence: a.alameri2222@gmail.com (A. A.);

Scopus Author ID 57194078029
Received: 17.01.2023; Accepted: 22.02.2023; Published: 3.02.2024

Abstract: The next-generation thermal fluid, that is, the hybrid nanofluids (hbnfs) are extensively used in numerous fields like industrial and manufacturing sectors as well as recent developments in biotechnology. Inspired by these applications, we investigated the argumentation of thermal energy transfer of AA7072 and AA7072 + AA7075 alloy nanoparticles (nps) suspended in H_2 O - based nanofluid and hybrid nanofluid flow past a non-linear porous stretching sheet. Thermal radiation, viscous dissipation, and heat source/sink are also studied in the modeling. The modeling PDEs are transmuted into ODEs by opting for appropriate similarity transformations. Furthermore, the transmuted equations are solved numerically in MATLAB using Runge-Kutta-Fehlberg's fourth-fifth order (RKF-45) technique by adopting the shooting method. The graphical representation is accomplished for important physical factors to check the behaviors of flow profiles. The velocity profile for AA7072 + AA7075/ H_2 O is higher than AA7072/ H_2 O. By increasing magnetic field parameter M and permeability parameter K_1, the velocity component (f^' (χ)), gain diminished trend for both AA7072/ H_2 O and AA7072 + AA7075/ H_2 O. The influence of Eckert number (Ec), and Heat source and sink parameter (Q) displays the rising trend in temperature profile for both nano and hybrid nanofluid. But the hybrid nanofluid is more effective when equated with nanofluid for both Ec, and Q. Moreover, the Dragging friction (Df), and Nusselt number (Nn) are also evaluated.

Keywords: hybrid nanofluid; porous stretching sheet; thermal radiation; heat source/sink.

1. Introduction

The next-generation thermal fluid is a hybridization of metal nps and metallic oxides, has enhanced heat transmission and rheological performance as well as exhibits superior thermophysical properties than base fluids (oil, water, ethylene glycol, or even an ionic liquid) and mono nanofluids. Recently, researchers indicated that an exhaustive mixture of several types of nps in base fluids can substantially improve the ability of fluid combinations. The thermal performance can be increased when more than one np is distributed in the base fluid. A plethora of literature has already been reported that hnf provides better heat transfer enhancement, it can be utilized in advanced thermal engineering applications such as solar energy, refrigeration as well as heating, ventilation, heat exchanger, coolant in machining and manufacturing, electronic cooling, automotive industry, generator cooling, nuclear system

cooling, biomedical, space, ships, and defense, etc. Firstly, Suresh *et al*. [1], identified the concepts of hnfs to improve on the effects of modern nanofluids using $Cu - Al_2O_3/water$ – based nps by hydrogen reduction technique. Santhi *et al*. [2], considered the slip conditions to evaluate the energy and thermal transfer rate of unsteady magnetohydrodynamic $Al_2O_3 - TiO_2/water$ – based hnf flow over a stretching surface inclusion of chemical reaction, suction, thermal radiation. The influence of volumetric heat generation and chemical reaction of higher order on MHD hnf across the bidirectional porous stretchable sheet was assessed by Joshi *et al*. [3]. Shanmugapriya *et al*. [4] depicted the heat and mass transport of magnetized $SWCNT + MWCNT/H_2O$ – based hnf over a moving wedge in the attendance of thermal radiation and activation energy with binary chemical reaction. Saeed *et al*. [5] examined the thermos physical characteristics of cylindrical-shaped carbon nanotubes (SWCNTs and MWCNTs) and Fe_3O_4 hnf of Darcy Forchheimer flow over an exponentially extending curved surface.

Nanomaterials are significant because of their immense thermal and mechanical properties. The physical properties of nanofluid formed by nanomaterials like metal and metallic oxides are noticeably altered by these materials. There is a new kind of nanomaterial known as Aluminum alloys (AAs) in which AAs play a predominant role in boosting thermal conductivity. AAs are widely utilized in the manufacturing of spacecraft, aircraft structures, construction, testing, transport utilization, etc. In addition, these AAs are acknowledged to have durable, demanding cool rates. Due to the high durability of AA7072 and AA7075 AAs, researchers explored the thermal transport behavior of hnf over various flow models. Abbasi *et al*. [6] analyzed the thermal transport of AA7072 and AA7075 AAs dispersed in methanol across the permeable plate with the effect of thermal and velocity slip, radiative heat flux, heat generation/absorption, and suction/injection. The slip effect of 3-D MHD flow of hnf across a stretched plane of non-uniform thickness was theoretically studied by Tlili *et al*. [7]. Utilizing a non-Fourier heat flux model, Madhukesh *et al*. [8] deliberated the impact of Newtonian heating (NH) and constant wall temperature (CWT) of AA7072-AA7075/water-based hnf over a curved stretching sheet. Some recent studies about AA7072-AA7075 AAs hnfs and thermal transport properties are mentioned in Refs. [9-11].

In an extremely high-temperature operating industry, the performance of thermal radiation plays a significant influence on the rate of heat transfer and temperature profiles. This potential leads to examining the impact of heat transfer on thermal radiation under the boundary layer flow problems. Furthermore, adding nps in a base fluid increases the fluid's thermal efficiency rate. Mahabaleshwar *et al*. [12] studied the analytical solution of thermal radiation of the hnf flow over a stretching/shrinking sheet with suction and injection. The investigation of hnf reported by Jaafar *et al*. [13] stated that the thickness of the thermal boundary layer increases as the increasing values of the magnetic and suction parameters. Asghar *et al*. [14], explored the influence of thermal hnf (alumina (Al_2O_3) and copper (Cu) nanoparticles) on the three-dimensional magnetized rotating flow with Joule heating. Based on the available literature, several researchers [15-20] did the dominant work applying the thermal radiation concept in their investigation.

A closer inquiry of the review literature, it is recognized that the thermal transport analysis of AA7072 and AA7072 + AA7075 alloy nps suspended in H_2O - based nanofluid and hnf are not recorded over a non-linear porous stretching sheet. Here, we considered two different AAs, AA7072 and AA7075, suspended in a base fluid H_2O. AA7072 alloy combines zinc and aluminum with additional metallic elements such as copper, silicon, and ferrous. The zinc content of 7072 aluminum increases its sacrificial anode property but has very poor

erosion-corrosion resistance. Similarly, one of the strongest aluminum alloys, AA7075 is a compounded mixture of zinc, magnesium, ferrous, copper, and silicon. For the novelty of the analysis, thermal radiation, viscous dissipation, and heat source/sink are ingrained in the present mathematical model. After that, a numerical method RKF-45 technique and shooting method are adopted to arrive at a solution. Through table and graphical illustrations, the results of velocity, temperature profiles, dragging friction, and Nusselt number for AA7072-H_2O and AA7072 + AA7075-H_2O are presented for various key parameters. This present study's contribution may benefit the development of industrial requirements, particularly in the process of household appliances, manufacturing sectors, and the recent developments in biotechnology.

2. Physical flow model formulation

The heat and mass transition is examined through 2D MHD, the steady incompressible flow of hnf past a non-linear porous stretching sheet. The hnf is composed of the mixture of alloy nps AA7072 and AA7072 + AA7075 suspended in H_2O. A physical flow structure of the problem is shown in Fig. 1, where the sheet moves with velocity $u_w(x) = ax^m$, depending on $a < 0\ or\ a > 0$ for shrinking or stretching sheets, respectively. A variable magnetic field $B(x) = B_0 x^{\frac{m-1}{2}}$ is applied normally to the non-linear stretching surface. The temperature of hnf far away from the non-linear stretching sheet is T_∞, whereas the hnf temperature at the sheet surface is T_w.

3. Model equations

The constitutive equations of the flow formulas of the MHD hbnf, with the effect of porous media, viscous dissipation, and thermal radiations, are defined as:

$$u_x + v_y = 0 \tag{1}$$

$$\rho_{hbnf}\left(uu_x + vu_y\right) = \mu_{hbnf}\left(u_{xx} - \frac{u}{K}\right) - \sigma B(x)^2 u \tag{2}$$

$$\left(\rho c_p\right)_{hbnf}(uT_x + vT_y) = \left(k_{hbnf} + \frac{16\sigma^* T_\infty^3}{3k^*}\right)T_{yy} + \mu_{hbnf}u_y^2 + Q'(T - T_\infty) \tag{3}$$

Associated border constraints are:

$$\left.\begin{array}{l} u|_{y=0} = u_w(x) = ax^m, v|_{y=0} = 0, T|_{y=0} = T_w(x) = T_\infty + bx^n \\ u|_{y=\infty} = 0, T|_{y=\infty} = T_\infty \end{array}\right\} \tag{4}$$

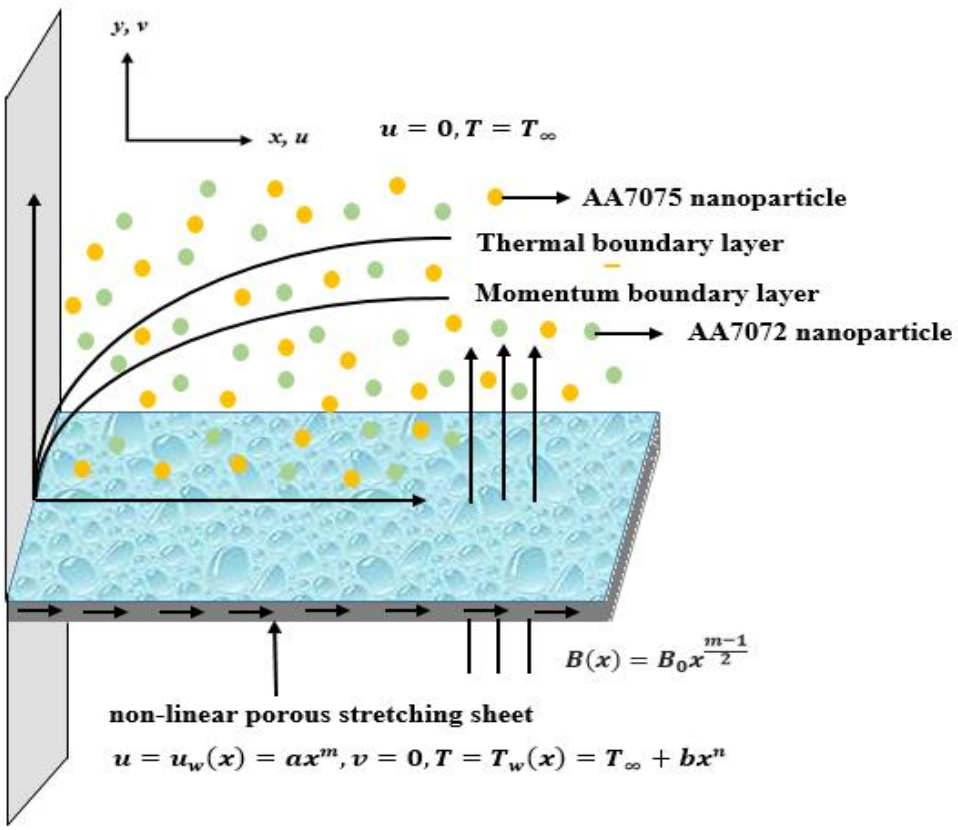

Figure 1. Flow model.

The dynamical viscidness model for hybrid nanofluid [4]:

$$\frac{\mu_{hbnf}}{\mu_{bf}} = \frac{1}{(1-\varphi_{\mathrm{AA7072}})^{2.5}(1-\varphi_{\mathrm{AA7075}})^{2.5}} \quad (5)$$

The density model for hybrid nanofluid:

$$\frac{\rho_{hbnf}}{\rho_{bf}} = \left[(1-\varphi_{\mathrm{AA7075}})\left\{(1-\varphi_{\mathrm{AA7072}}) + \varphi_{\mathrm{AA7072}}\frac{\rho_{\mathrm{AA7072}}}{\rho_{bf}}\right\} + \varphi_{\mathrm{AA7075}}\frac{\rho_{\mathrm{AA7075}}}{\rho_{bf}}\right] \quad (6)$$

The consistent heat capability model for hybrid nanofluid:

$$\frac{(\rho c_p)_{hbnf}}{(\rho c_p)_{bf}} = \left[(1-\varphi_{\mathrm{AA7075}})\left\{(1-\varphi_{\mathrm{AA7072}}) + \varphi_{\mathrm{AA7072}}\frac{(\rho c_p)_{\mathrm{AA7072}}}{(\rho c_p)_{bf}}\right\} + \varphi_{\mathrm{AA7075}}\frac{(\rho c_p)_{\mathrm{AA7075}}}{(\rho c_p)_{bf}}\right] \quad (7)$$

The thermal conductivity model for hybrid nanofluid:

$$\left.\begin{aligned}\frac{k_{hbnf}}{k_{nf}} &= \left[\frac{k_{\mathrm{AA7075}} + 2k_{nf} - 2\varphi_{\mathrm{AA7075}}(k_{nf} - k_{\mathrm{AA7075}})}{k_{\mathrm{AA7075}} + 2k_{nf} + \varphi_{\mathrm{AA7075}}(k_{nf} - k_{\mathrm{AA7075}})}\right], \\ \frac{k_{nf}}{k_{bf}} &= \left[\frac{k_{\mathrm{AA7072}} + 2k_{bf} - 2\varphi_{\mathrm{AA7072}}(k_{bf} - k_{\mathrm{AA7072}})}{k_{\mathrm{AA7072}} + 2k_{bf} + \varphi_{\mathrm{AA7072}}(k_{bf} - k_{\mathrm{AA7072}})}\right]\end{aligned}\right\} \quad (8)$$

where $\mu_{bf}, \rho_{bf}, (\rho c_p)_{bf}$ and k_{bf} are the dynamical viscidness, density, consistent heat capability, and thermal conductivity of the base fluid. φ is the volume fraction of the alloy nps. The physical assets of AA7072 and AA7075 aluminum alloys and H_2O are tabulated in Table 1.

Table 1. Alloy nps and H_2O thermophysical assets [18].

Thermophysical Characteristics	Unit	Base fluid	Nanomaterials	
		H_2O	AA7072	AA7075
$\boldsymbol{\rho}$	kg/m^3	997.1	2810	2720
$\boldsymbol{c_p}$	J/kgK	4179	960	893
$\boldsymbol{k}$	W/mK	0.613	173	222

4. Dimensionless formulations model

The similarity technology used in Equations (1) – (4) are as follows:

$$\psi(x,y) = \left(\frac{2a\vartheta_{bf}}{m+1}\right)^{\frac{1}{2}} x^{\frac{m+1}{2}} f(\chi), \qquad \chi(x,y) = y\left(\frac{a(m+1)}{2\vartheta_{bf}}\right)^{\frac{1}{2}} x^{\frac{m-1}{2}}, \theta(\chi) = \frac{T-T_\infty}{T_w-T_\infty} \tag{9}$$

By incorporating Equation (9), we get:

$$f''' - \frac{\varphi_B}{\varphi_A}\left[\left(\frac{2m}{m+1}\right)f'^2 - ff''\right] - \frac{1}{\varphi_A}Mf' - K_1 f' = 0 \tag{10}$$

$$\left[1+\frac{R}{\varphi_D}\right]\theta'' - \frac{Pr}{\varphi_A}\left[\varphi_C\left(\frac{4m}{m+1}\right)f'\theta - \varphi_C f\theta' - Q\theta - \varphi_A\varphi_C Ec(f'')^2\right] = 0 \tag{11}$$

here $\varphi_A = \frac{\mu_{hbnf}}{\mu_{bf}}, \varphi_B = \frac{\rho_{hbnf}}{\rho_{bf}}, \varphi_C = \frac{(\rho c_p)_{hbnf}}{(\rho c_p)_{bf}}, \varphi_D = \frac{k_{hbnf}}{k_{bf}}$.

The translated border constraints are:

$$f|_{\chi=0} = 0, f'|_{\chi=0} = 1, \theta|_{\chi=0} = 1, f'|_{\chi\to\infty} = 1, \theta|_{\chi\to\infty} = 0. \tag{12}$$

The default value and the description of the control physical parameters embedded in equations (10) and (12) are given in Table 2.

Table 2. Default value and the description of the control physical parameters

Physical parameters	Expression	Name	Default value
$\boldsymbol{m}$	-	non-linear stretching parameter	0.2
$\boldsymbol{M}$	$\frac{2\sigma B_0^2}{a(m+1)\rho_{bf}}$	Magnetic parameter	0.5
$\boldsymbol{R}$	$\frac{16\sigma^* T_\infty^3}{3k^* k_{bf}}$	Radiation parameter	1.0
$\boldsymbol{Ec}$	$\frac{u_w^2}{(c_p)_{bf}(T_w-T_\infty)}$	Eckert number	0.5
$\boldsymbol{Q}$	$\frac{2Q_0}{a(m+1)(\rho c_p)_{bf}}$	Heat source and sink parameter	0.5
$\boldsymbol{Pr}$	$\frac{\gamma_{bf}}{\alpha_{bf}}$	Prandtl number	6.2
$\boldsymbol{K_1}$	$\frac{2\gamma_{bf}}{Ka(m+1)x^{m-1}}$	Permeability parameter	0.2
$\boldsymbol{\varphi_{AA7075}}$	-	volumetric fraction parameter of $AA7075$	0.2
$\boldsymbol{\varphi_{AA7072}}$	-	volumetric fraction parameter of $AA7072$	0.2

5. Dragging friction and Nusselt number

The dragging friction S_{fx} combined with the Nusselt amount H_{tx} are the interesting physical quantities that controlled the hybrid nanofluid fluid and specified as:

$$S_{fx} = \frac{\tau_w}{\rho_{bf}\left(u_w(x)\right)^2},$$
$$H_{tx} = \frac{x q_w}{k_{bf}(T_w - T_\infty)} \quad (13)$$

where

$$\tau_w = \mu_{hbnf}\left.\frac{\partial u}{\partial y}\right|_{\chi=0}, q_w = -\left[k_{hbnf}\left.\frac{\partial T}{\partial y}\right|_{\chi=0} + \frac{16\sigma^*}{3k^*}\left(T_\infty^3 \frac{\partial T}{\partial y}\right)\right|_{\chi=0}\Bigg] \quad (14)$$

The dimensionless translation of Eq. (13) is as follows:

$$\left.\begin{aligned} S_{fx}(Re_x)^{0.5} &= \frac{1}{(1-\varphi_{\mathrm{AA7075}})^{2.5}(1-\varphi_{\mathrm{AA7072}})^{2.5}}\sqrt{\frac{m+1}{2}}f''(0) \\ H_{tx}(Re_x)^{-0.5} &= -\frac{k_{hbnf}}{k_{bf}}\sqrt{\frac{m+1}{2}}[1+R]\theta'(0) \end{aligned}\right\} \quad (15)$$

where $Re_x = \frac{ax^{m+1}}{\vartheta_{bf}}$ is the local Reynolds number.

6. Numerical Procedure and validation

Equations (10) and (11), along with border constraints (12), are solved utilizing the shooting technique together with $RKF45$ method by converting BVP into an IVP [17]. At the initial stage,

$$f''' = \frac{\varphi_B}{\varphi_A}\left[\left(\frac{2m}{m+1}\right)f'^2 - ff''\right] + \frac{1}{\varphi_A}Mf' + K_1 f' \quad (16)$$

$$\theta'' = \frac{1}{\left[1+\frac{R}{\varphi_D}\right]}\left[\frac{Pr}{\varphi_A}\left[\varphi_C\left(\frac{4m}{m+1}\right)f'\theta - \varphi_C f\theta' - Q\theta - \varphi_A\varphi_C Ec(f'')^2\right]\right] \quad (17)$$

Introducing the new variables as:

$$\xi_1 = f, \quad \xi_2 = f', \quad \xi_3 = f'', \quad \xi_4 = \theta, \quad \xi_5 = \theta' \quad (18)$$

The matrix form of the governing equations with $\xi = [f, f', f'', \theta, \theta']^T$ can be written as follows:

$$\frac{d}{d\chi}\begin{pmatrix}\xi_1\\ \xi_2\\ \xi_3\\ \xi_4\\ \xi_5\end{pmatrix} = \begin{pmatrix}\xi_2\\ \xi_3\\ \frac{\varphi_B}{\varphi_A}\left[\left(\frac{2m}{m+1}\right)\xi_2{}^2 - \xi_1\xi_3\right] + \frac{1}{\varphi_A}M\xi_2 + K_1\xi_2\\ \xi_5\\ \frac{1}{\left[1+\frac{R}{\varphi_D}\right]}\left[\frac{Pr}{\varphi_A}\left[\varphi_C\left(\frac{4m}{m+1}\right)\xi_2\xi_4 - \varphi_C\xi_1\xi_5 - Q\xi_4 - \varphi_A\varphi_C Ec\left(\xi_3\right)^2\right]\right]\end{pmatrix} \quad (19)$$

with

$$\left.\begin{aligned}&\xi_1|_{\chi=0} = 0, \xi_2|_{\chi=0} = 1, \xi_2|_{\chi=0} = 1,\\ &\xi_3|_{\chi\to\infty} = \alpha_1, \xi_2|_{\chi\to\infty} = \alpha_2.\end{aligned}\right\} \quad (20)$$

where α_1 and α_2 are unknowns. Initially, the shooting technique is implemented to get an initial guess value for unknowns. Then, the captured IVP Eqs. (19 - 20) are solved numerically by using the RKF-45 method. To aggravate the validation of the analysis, the obtained results are compared to those from previous studies, resulting in similar findings (see Tables 3 and 4).

Table 3. Computational values of $f''(0)$ for various m in the absence of $\varphi_1, \varphi_2, M, and\ K_1 = 0$

m	**Cortell [19]**	**Elayarani *et al.* [20]**	**Present work**
0	0.6276	0.62779	0.6276
0.2	0.7668	0.76705	0.7668
0.5	0.8895	0.88974	0.8895
1	1.0000	1.00017	1.0000
3	1.1486	1.14874	1.1486
10	1.2349	1.23501	1.2349
20	1.2574	1.25755	1.2574

Table 4. Computational values of $\theta'(0)$ for various m and Ec in the absence of $\varphi_1, \varphi_2, M, Q, R\ and\ K_1 = 0, and\ Pr = 1$

Ec	***m***	**Eldabe *et al.* [21]**	**Elayarani *et al.* [20]**	**Present work**
0	0.75	1.25270	1.25272	1.25267
0	1.5	1.43937	1.43936	1.43939
0	7.0	1.69930	1.69928	1.69929
0	10.0	1.72894	1.72891	1.72893
0.1	0.75	1.21994	1.21994	1.21998
0.1	1.5	1.40515	1.40515	1.40508
0.1	7.0	1.66257	1.66254	1.66250
0.1	10	1.69188	1.69185	1.69182

7. Graphical Results

This section highlights the physical mechanism and trend of velocity and thermal fields behind each figure.

8. Velocity field

The influences of m on the velocity field $(f'(\chi))$, for AA7072-H_2O and AA7072 + AA7075-H_2O nanofluid and hnf are plotted in Figure 2. The upsurge in the m value declines the $f'(\chi)$ for all two cases. To see the influence of magnetic parameter M on $f'(\chi)$, results are drawn in Figure 3. This figure talks about the velocities of both AA7072-H_2O and AA7072 + AA7075-H_2O nanofluid and hnf decline near the convective surface, and these variations are almost insignificant for both types of fluids. The velocities of AA7072-H_2O nanofluid is rapid decrement as compared to that of AA7072 + AA7075-H_2O hnf. The volumetric fraction parameters $\varphi_{\mathrm{AA7075}}$ and $\varphi_{\mathrm{AA7075}}$ plays an important role in the study of hnf. To analyze the influence of volumetric fraction parameters on $f'(\chi)$, Figures 4 and 5 are depicted. Here, the arguments of φ_1 and φ_2 improves the velocities of both cases. For AA7072 + AA7075-H_2O hnf, dominating behavior of AA7072-H_2O nanofluid is observed. Figure 6 shows the influence of K_1on $f'(\chi)$. Increasing K_1 values decline the velocity profile for both cases.

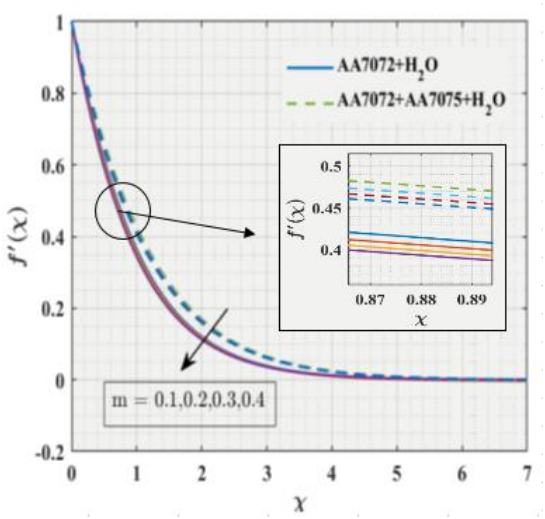

Figure 2. Influence of m for $f'(\chi)$.

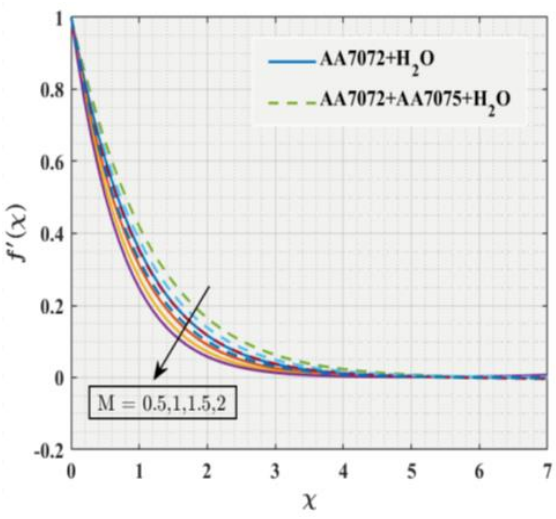

Figure 3. Influence of M for $f'(\chi)$.

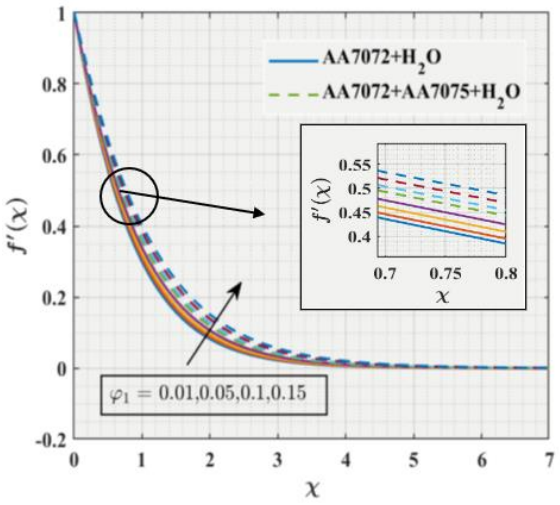

Figure 4. Influence of φ_1 for $f'(\chi)$.

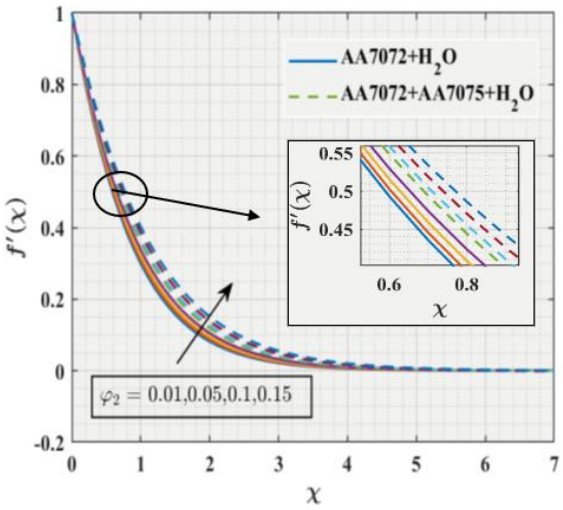

Figure 5. Influence of φ_2 for $f'(\chi)$.

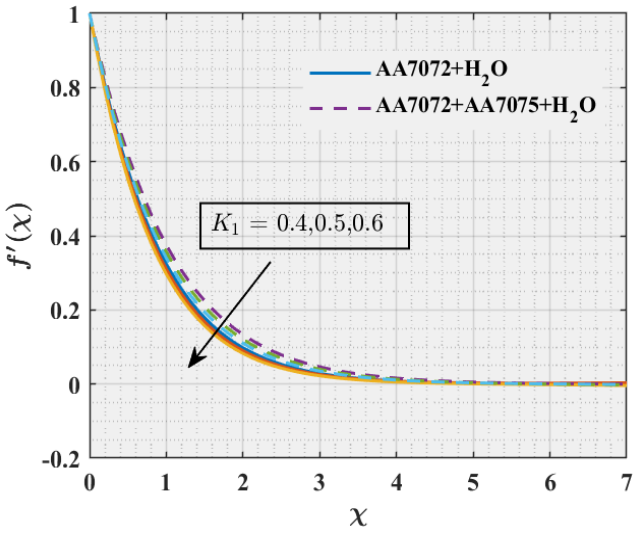

Figure 6. Influence of K_1 for $f'(\chi)$.

9. Thermal field

The impact of non-dimensional physical parameters on the temperature profile of AA7072-H_2O and AA7072 + AA7075-H_2O nanofluid and hnf are illustrated in Figures 7–15. We captured from Figure 7, for improvement in m, temperature for both AA7072-H_2O and AA7072 + AA7075-H_2O nanofluid and hnf rise near the stretchable surface, that is, at $\eta = 0\ to\ \eta = 1.5$, after the thermal field slows down. The fluctuation in the temperature profile for varied values of M is illustrated in Figure 8. The plotted figure shows that for stronger magnetic parameters AA7072 + AA7075-H_2O hybrid nanofluid has a better thermal field than the AA7072-H_2O nanofluid. Variation in $\theta(\chi)$ against φ_1 and $\varphi_2$for both cases is portrayed in Figures 9 and 10. Due to high thermal conductivity, the temperature profile of both fluids starts increasing, beyond $\eta \geq 1.5$, the temperature profile decreases asymptotically for both cases. The impact of Pr on the thermal field is represented in Figure 11. The enhanced Pr values reduce the AA7072-H_2O and AA7072 + AA7075-H_2O nanofluid and hnf temperature because the higher Pr values retain lower thermal conductivity. One can observe from plotted Figure 12 that the upsurge in radiation parameter declines the thermal field. The behavior of the temperature profile with the increment of the Eckert number is displayed in Figure 13. The heat capacitance of AA7075 aluminum alloy nps is greater than AA7072 AA np. Because for AA7075 alloy nps, the temperature profile of AA7072 + AA7075-H_2O hnf rises compared to AA7072-H_2O nanofluid. The stimuli of heat source/sink parameter on thermal characteristics of AA7072-H_2O and AA7072 + AA7075-H_2O are plotted in Figure 14. For raising values of Q, the dominant effects of temperature profile are observed for hnf compared to that of nanofluids. Figure 15 reveals the impact of the permeability parameter on the thermal field for two different fluids. The rate of declination in the thermal field is slower for hnf when compared to nanofluid.

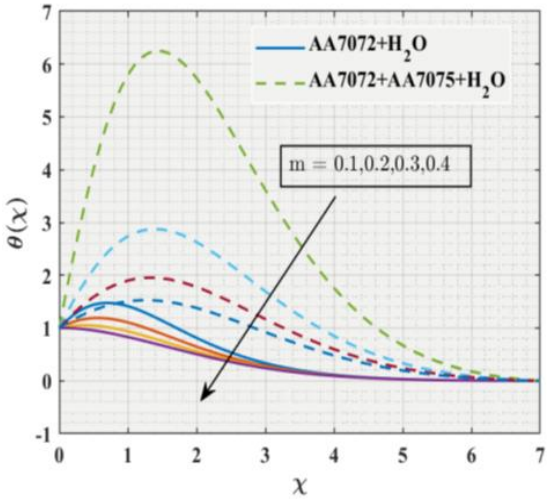

Figure 7. Influence of m for $\theta(\chi)$.

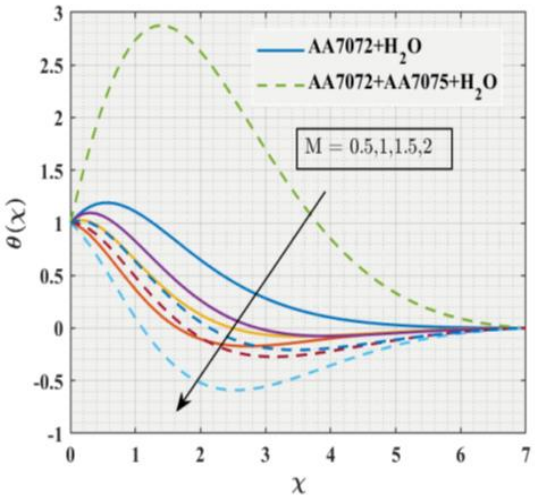

Figure 8. Influence of M for $\theta(\chi)$.

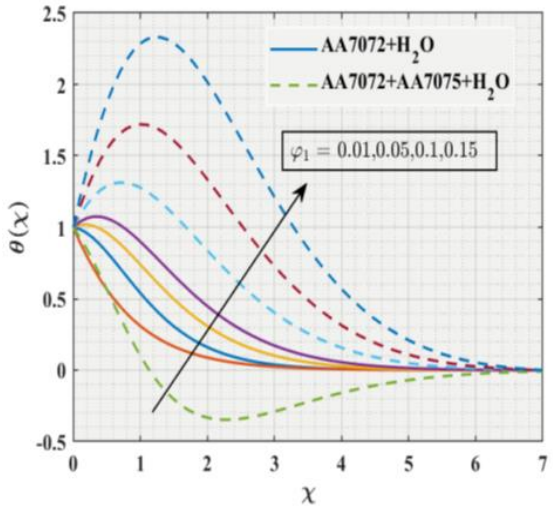

Figure 9. Influence of φ_1 for $\theta(\chi)$.

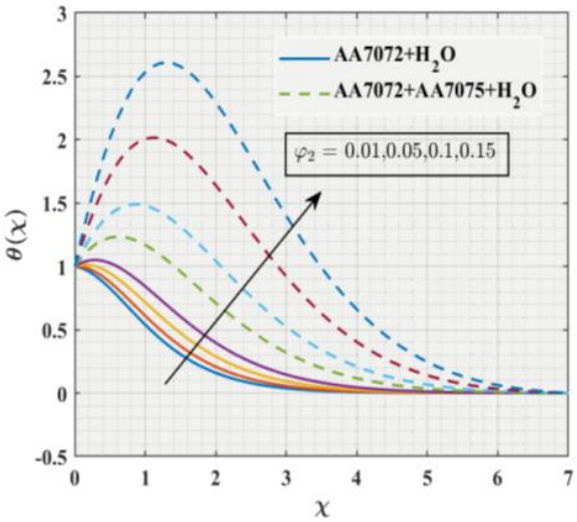

Figure 10. Influence of φ_2 for $\theta(\chi)$.

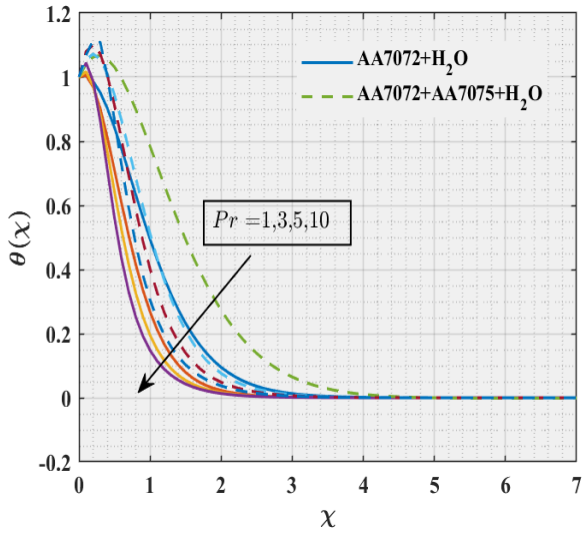

Figure 11. Influence of Pr for $\theta(\chi)$.

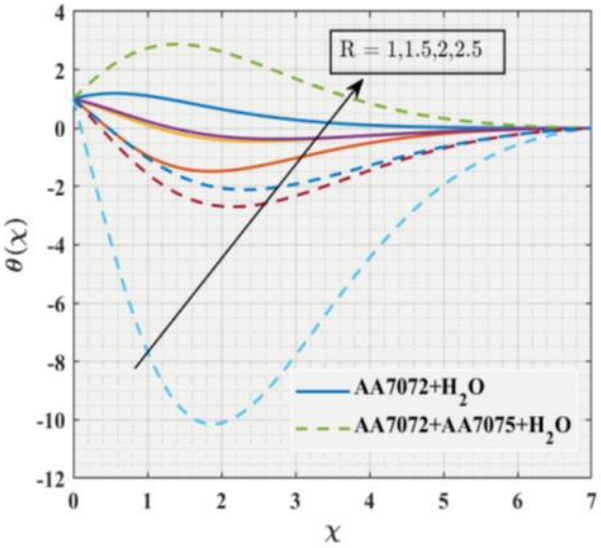

Figure 12. Influence of R for $\theta(\chi)$.

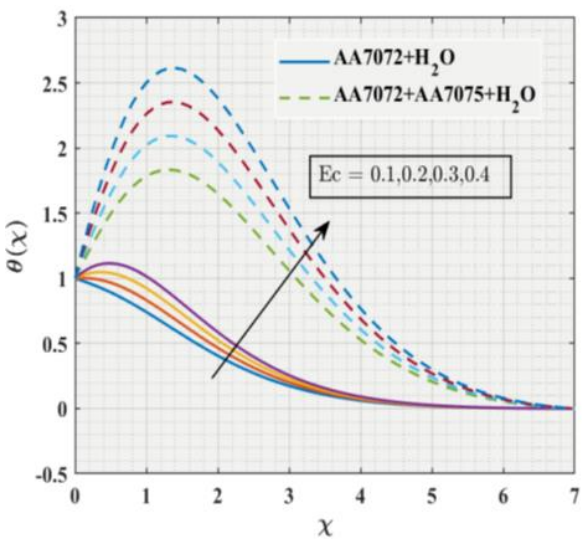

Figure 13. Influence of Ec for $\theta(\chi)$.

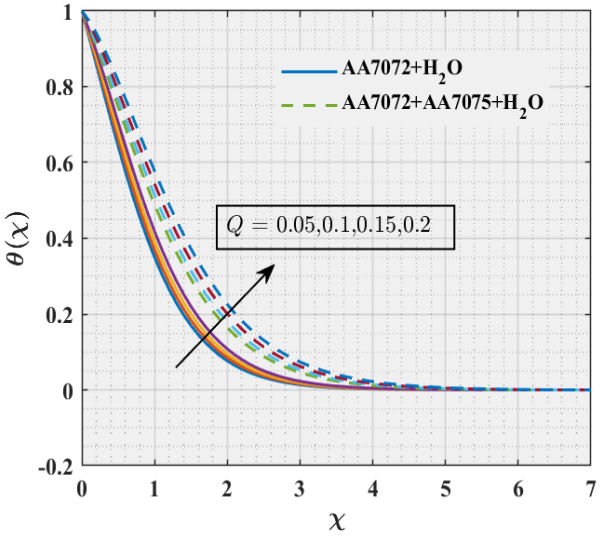

Figure 14. Influence of Q for $\theta(\chi)$.

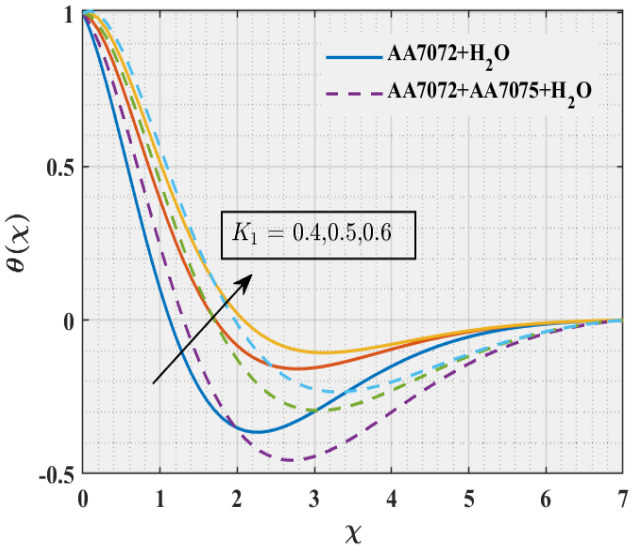

Figure 15. Influence of K_1 for $\theta(\chi)$.

10. Conclusions

2-D MHD hnf with AA7072 and AA7075 aluminum alloy nps, thermal radiation, and heat source/sink are defined in this present work. The numerical results of the simulated problem were accomplished using the RKF-45 technique together with the shooting method. The following are some of the most significant aspects of the results:

Velocity field under the influence of growing non-linear stretching parameter (m), magnetic parameter (M), and permeability parameter (K_1), behaves in the opposite manner in AA7072-H_2O and AA7072 + AA7075-H_2O nanofluid and hybrid nanofluid.

Irrespective of the volumetric fraction parameter of $AA7075$ (φ_{AA7075}), and volumetric fraction parameter of $AA7072$ (φ_{AA7072}), $f'(\chi)$ has a higher magnitude for all nanofluid and hybrid nanofluid.

Enhanced Eckert number (Ec), heat source and sink parameter (Q), and permeability parameter (K_1) causes $\theta(\chi)$ to grow while that of radiation parameter (R) declines for both types of AA7072-H_2O and AA7072 + AA7075-H_2O nanofluids.

Hiked φ_{AA7075} and φ_{AA7072} contributes greater dragging friction (S_{fx}) in both nanofluids while rising in m, M and K_1 leads to the decay of viscous drag in both types of nanofluids.

The rate of heat transfer (H_{tx}) increases due to hybridity and also with an increment of volume fraction parameters φ_{AA7075}, φ_{AA7072}, Ec, Q and K_1 for nanofluid and hybrid nanofluid.

Funding

This research received no external funding.

Acknowledgments

The authors wish to thank the anonymous reviewers in advance.

Conflicts of Interest

The authors declare that they have no conflict of interest.

References

1. Suresh, S.; Venkitaraj, K.P.; Selvakumar, P.; Chandrasekar, M. Synthesis of Al_2O_3–Cu/water hybrid nanofluids using two step method and its thermo physical properties, *Colloids and Surfaces A: Physicochemical and Engineering Aspects*, **2011**, *388*, , 41-48, http://dx.doi.org/10.1016/j.colsurfa.2011.08.005
2. Santhi, M.; Suryanarayana Rao, K. V.; Sudarsana Reddy, P.; Sreedevi, P. Heat and mass transfer characteristics of radiative hybrid nanofluid flow over a stretching sheet with chemical reaction. *Heat Transfer*, **2020**, 1–21, http://dx.doi.org/10.1002/htj.22012
3. Joshi, N.; Upreti, H.; Pandey, A.K.; Manoj, Kumar. Heat and Mass Transfer Assessment of Magnetic Hybrid Nanofluid Flow via Bidirectional Porous Surface with Volumetric Heat Generation, *International Journal of Applied and Computational Mathematics*,**2021**, *7*, 1-17, https://link.springer.com/article/10.1007/s40819-021-00999-3
4. Shanmugapriya, M.; Sundareswaran, R.; Senthil Kumar, P. Heat and Mass Transfer Enhancement of MHD Hybrid Nanofluid Flow in the Presence of Activation Energy", *International Journal of Chemical Engineering*, **2021,** 1-12. Article ID 9473226, http://dx.doi.org/10.1155/2021/9473226
5. Saeed, A.; Alghamdi, W.; Mukhtar, S.; Shah SIA, Kumam P.; Gul T, *et al*. Darcy-Forchheimer hybrid nanofluid flow over a stretching curved surface with heat and mass transfer, *PLoS ONE*, **2021**, *16*, e0249434, http://dx.doi.org/10.1371/journal.pone.0249434
6. Adnan, Ullah Khan, S.I.; Khan, U.; Ahmed, N.; Mohyud-Din, S. T.; Khan, I.; Nisar, K. S. Thermal transport investigation in AA7072 and AA7075 aluminum alloys nanomaterials based radiative nanofluids by considering the multiple physical flow conditions. *Scientific Reports*, **2021**, *11***,** 9837, https://www.nature.com/articles/s41598-021-87900-w
7. Tlili, I.; Nabwey, H.A.; Ashwinkumar, G.P.; and Sandeep, N. 3-D magnetohydrodynamic AA7072-AA7075/methanol hybrid nanofluid flow above an uneven thickness surface with slip effect. *Scientific Reports*, **2020,** *10***,** 4265, https://www.nature.com/articles/s41598-020-61215-8
8. Mahabaleshwar, U.S.; Vishalakshi, A.B.; Helge I. Andersson. Hybrid nanofluid flow past a stretching/shrinking sheet with thermal radiation and mass transpiration, *Chinese Journal of Physics*, **2022,** *75*, 152-168, http://dx.doi.org/10.1016/j.cjph.2021.12.014
9. Shah, Z.; Vrinceanu, N.; Rooman, M.; Deebani, W.; Shutaywi, M. Mathematical Modelling of Ree-Eyring Nanofluid Using Koo-Kleinstreuer and Cattaneo-Christov Models on Chemically Reactive AA7072-AA7075 Alloys over a Magnetic Dipole Stretching Surface, *Coatings*, **2022,** *12*, 391, http://dx.doi.org/10.3390/coatings12030391

10. Salahuddin, T.; Abdul, M. B.; Mair Khan; Basem Al Alwan; Mohammad A. Hybrid nanofluid analysis for a class of alumina particles, *Chinese Journal of Physics*, **2022**, *77*, 2550-2560, http://dx.doi.org/10.1016/j.cjph.2021.11.012
11. Salahuddin, T.; Nazim, S.; Mair, K.; Yu–Ming Chu. A hybrid nanofluid flow near a highly magnetized heated wavy cylinder, *Alexandria Engineering Journal*, **2022,** *61*, 1297-1308, http://dx.doi.org/10.1016/j.aej.2021.06.014
12. A'isyah, J.; Iskandar W.; Anuar, J.; Roslinda, N.; Ioan Pop. MHD flow and heat transfer of a hybrid nanofluid past a non-linear surface stretching/shrinking with effects of thermal radiation and suction, *Chinese Journal of Physics*. **2022,** *79*, 13-27, http://dx.doi.org/10.1016/j.cjph.2022.06.026
13. Asghar, A.; Lund, L.A.; Shah, Z.; Vrinceanu, N.; Deebani, W.; Shutaywi, M. Effect of Thermal Radiation on Three-Dimensional Magnetized Rotating Flow of a Hybrid Nanofluid. *Nanomaterials*, **2022**, *12*, 1566, http://dx.doi.org/10.3390/nano12091566
14. Roşca, N.C.; Roşca, A.V.; Pop, I. Axisymmetric flow of hybrid nanofluid due to a permeable non-linearly stretching/shrinking sheet with radiation effect. *International Journal of Numerical Methods for Heat & Fluid Flow*, **2021,** *31*, 2330–2346, http://dx.doi.org/10.1108/HFF-09-2020-0574
15. Shoaib, M.; Raja, M.A.Z.; Sabir, M.T.; Islam, S.; Shah, Z.; Kumam, P.; Alrabaiah, H. Numerical investigation for rotating flow of MHD hybrid nanofluid with thermal radiation over a stretching sheet. *Scientific Reports*, **2020**, *10*, 1–15, http://dx.doi.org/10.1038/s41598-020-75254-8
16. Eid, M.R.; Nafe, M.A. Thermal conductivity variation and heat generation effects on magneto-hybrid nanofluid flow in a porous medium with slip condition. *Waves Random Complex Media*, **2020,** 1–25, http://dx.doi.org/10.1080/17455030.2020.1810365
17. Gopi Krishna, S.; Shanmugapriya, M.; SundareswaranR.; Senthil Kumar, P. MANFIS approach for predicting heat and mass transport of bio-magnetic ternary hybrid nanofluid using Cu/Al2O3/MWCNT nanoadditives. *biomass conversion and biorefinery*, **2022**, 1-16, http://dx.doi.org/10.1007/s13399-022-02989-x
18. Khan U, Zaib, A.; Abu Bakar, S.; Ishak, A. Forced convection flow of water conveying AA7072 and AA7075 alloys-nanomaterials on variable thickness object experiencing Dufour and Soret effects. *Scientific Repoprt*, **2022**, *12*, 6940, http://dx.doi.org/10.1038/s41598-022-10901-w
19. Cortell, R. Heat and fluid flow due to non-linearly stretching surfaces, *Applied Mathematics and Computation* **2011**, *217*, pp. 7564-7572, http://dx.doi.org/10.1016/j.amc.2011.02.029
20. Elayarani, M.; Shanmugapriya, M.; Senthil Kumar, P. Estimation of magnetohydrodynamic radiative nanofluid flow over a porous non-linear stretching surface: application in biomedical research, *IET Nanobiotechnology*, **2019,** *13*, 911-922, http://dx.doi.org/10.1049/iet-nbt.2018.5427